J Therm Anal Calorim (2013) 111:93–99
DOI 10.1007/s10973-011-2185-2

Thermal degradation pathways of nickel(II) bipyridine complexes to size-controlled nickel nanoparticles

Nadia Parveen · Rabia Nazir · Muhammad Mazhar

Received: 24 October 2011 / Accepted: 21 December 2011 / Published online: 26 January 2012

Abstract Tris(bipyridine)nickel(II) chloride (**1**) and bis(bipyridine)nickel(II) chloride (**2**) pyrolize at heating rate of 50 °C/min to a maximum of 450 °C for 24 h under an inert atmosphere of flowing argon gas, to yield size-controlled nickel nanoparticles. Thermogravimetric studies of the complexes (**1**) and (**2**) and GC–MS analysis of the trapped volatile matter evolved during thermal degradation of the complexes indicate their clean decomposition pathway to zero-valent nickel. Both heating rate and argon gas flow rate affect purity, particle size, and shape of the particles. X-ray powder diffractometry and atomic force microscopy showed the formation of face-centered cubic (*fcc*) structured nickel particles having particle size in the range of 3.5–5.0 nm. Magnetic susceptibility measurements suggest nickel nanoparticles to be ferromagnetic in nature characterized by particle size–dependent Curie temperature and high coercivity that is comparable to the bulk iron.

Keywords Bipyridine nickel(II) · Pyrolysis · Nickel nanoparticles · Mechanism

N. Parveen
Department of Chemistry, Quaid-i-Azam University, Islamabad 45320, Pakistan

R. Nazir
Applied Chemistry Research Centre, PCSIR Laboratories Complex, Lahore 54600, Pakistan

M. Mazhar (✉)
Department of Chemistry, University of Malaya, 50603 Kualalampur, Malaysia
e-mail: mazhar42pk@yahoo.com

Introduction

Since past few decades, there has been substantial concern on the synthesis of magnetic nanoparticles (NPs) because of their extended properties and vital applications in various fields of life [1–4]. Among these, nickel NPs have recently been a focus of intense research owing to their use in magnetic sensors, memory devices [5], and catalysis [6–8]. Different methods like chemical reduction [9], sol–gel [10], microemulsion [11, 12], reverse microemulsion [13], hydrogen plasma method [14], solution reduction method [8], pulsed-laser ablation [15], and polyol process [16] have been generally used for the synthesis of Ni NPs. However, all these methods are costly and adsorption of surfactants on the surface of NPs is a frequent problem, which confines their effectiveness for specific applications [17]. In addition to that, Ni NPs are easily prone to oxidation [13, 18]. To avoid this problem, the use of organometallic precursors like $Ni(CO)_4$, $Ni(Cp)_2$, and $Ni(COD)_2$ has been proven interesting for synthesis of Ni NPs [19], but these precursors are highly toxic in nature [20].

Since the methods of preparation and experimental conditions have an obvious effect on dimensions, morphology, and surface properties of NPs, therefore compared with conventional methods, a much reasonable and competent thermal decomposition approach to produce stable monodispersed NPs is currently gaining attention [21–23]. Using this approach, Ni NPs were synthesized by thermal decomposition of Ni–oleate complex under inert gas flow [24]. *fcc* and *hcp* Ni NPs have also been successfully prepared via thermal decomposition of nickel(II)acetyl acetone [25], nickel acetate tetrahydrate [21, 26], and nickel(II)hydroxoacetophenato [18] using alkylamine as stabilizer. But relatively complicated reaction media due to the use of surfactants and stabilizers and time-to-time

temperature programing make the synthetic procedures followed, less valuable. The surface properties of NPs are also affected owing to capping by stabilizers used [18].

The focus of the present effort is to offer a comparatively simpler method for the production of stable Ni NPs via thermally decomposing bipyridine complexes of nickel(II) chloride at 450 °C under argon gas flow without using any surfactant or stabilizer. The mechanism of thermal decomposition of the complexes to Ni NPs has also been worked out.

Experimental details

Materials

All the reagents used in this study are of analytical grade and were used without further purification. Nickel(II) chloride hexahydrate and 2,2′-bipyridine were purchased from Aldrich and used as received.

Synthesis of $[Ni(2,2'\text{-bipy})_3]Cl_2{\cdot}5H_2O$ (**1**) and $[Ni(2,2'\text{-bipy})_2Cl_2]$ (**2**)

$[Ni(2,2'\text{-bipy})_3]Cl_2{\cdot}5H_2O$ (**1**) and $[Ni(2,2'\text{-bipy})_2Cl_2]$ (**2**) were prepared by following the reported methods [27, 28]. The prepared complexes were confirmed by characterizing them using elemental analysis, UV/Vis spectroscopy, FT-IR, ^{1}H-NMR, and mass spectrometry.

*$[Ni(2,2'\text{-bipy})_3]Cl_2{\cdot}5H_2O$ (**1**)*

Yield: 86%. Decomp. Point: 166 °C. λ_{max} (Ethanol) Found (Reported): 534 nm (542 nm) [27]. Elemental analysis calculated for $C_{36}H_{40}Cl_2NiO_5$ (MW = 682): Calculated (Found): C: 50.89% (51.01%); H: 4.87% (5.10%); N: 11.95% (11.90%). IR (cm^{-1}): ν(C–H_{arom}) 3073; ν(C–N_{arom}) 1598; ν(C–C_{arom}) 1441–1642; ν(Ni–N) 436. ^{1}H-NMR (DMSO-d_6, ppm): 7.45 (1H, t); 7.94 (1H, t); 8.37 (1H, d); 8.68 (1H, d). FAB: m/z 527 ($[Ni(bipy)_3]^+$), m/z = 405 ($[Ni(bipy)_2Cl]^+$), m/z = 370 ($[Ni(bipy)_2]^+$), m/z = 214 ($[Ni(bipy)]^+$), m/z = 183 ($[Ni(bipy)_{0.34}Cl_2]$), m/z = 157 ($[bipyH]^+$).

*$[Ni(2,2'\text{-bipy})_2Cl_2]$ (**2**)*

Yield: 87%. m.p: stable up to 320 °C. λ_{max} (Ethanol) Found (Reported): 600 nm (605 nm) [28]. Elemental analysis calculated for $C_{24}H_{20}Cl_2Ni$ (MW = 438): Calculated (Found): C: 54.10% (54.34%), H: 3.72% (3.62%), N: 11.88% (12.68%). IR (cm^{-1}): ν(C–H_{arom}) 3047; ν(C–N_{arom}) 1598; ν(C–C_{arom}) 1440–1573; ν(Ni–N) 438; ν(Ni–Cl) 272. ^{1}H NMR (DMSO-d_6, ppm): 7.43 (1H, s); 7.92 (1H, s); 8.36 (1H, s); 8.66 (1H,s). FAB: m/z = 405 ($[Ni(bipy)_2Cl]^+$), m/z = 370 ($[Ni(bipy)_2]^+$), m/z = 214 ($[Ni(bipy)]^+$), m/z = 183 ($[Ni(bipy)_{0.34}Cl_2]$), m/z = 157 ($[bipyH^+]$).

Synthesis of Ni(0) nanoparticles

About 1.23 g of each of the complex (**1**) and (**2**) was taken separately in alumina boat. The boat was then placed in a tube furnace connected to an argon gas supply line. The gas outlet of furnace was attached in series to pre-evacuated Schlenk tube, ethanol trapper, and silver nitrate (1 M) solution bath in order to collect/trap the evolved gas coming out as decomposition products for further analysis. The temperature of furnace was raised to 450 °C at the heating rate of 50 °C/min keeping argon gas flow rate at 1 L/min. Contents were kept at 450 °C for 24 h and then allowed to cool to room temperature under inert atmosphere to result in Ni NPs (Ni-1 from complex (**1**) and Ni-2 from complex (**2**), respectively). Yield was 80–85%.

Characterization

The Ni(II) bipyridine complexes (**1**) and (**2**) were characterized using elemental analysis, UV/Vis spectroscopy, FT-IR, ^{1}H-NMR, and mass spectrometry. Elemental analysis was performed on CHNS-932 Leco, USA. The UV–Vis spectra were recorded on UV-1700. ^{1}H-NMR analysis was obtained using Bruker 300 MHz NMR. TG and FT-IR studies were made on TGA/SDTA 851e, Metller Toledo, Swiss. Evolved gases trapped during thermal decomposition process were analyzed using Agilent GC–MS model 6890N.

Ni NPs (Ni-1 and Ni-2) obtained via thermal decomposition of bipyridine complexes (**1**) and (**2**), respectively, were analyzed using CHN, XRPD, EDX, AFM, and magnetic susceptibility. EDX was recorded on Leo 1530VP having accelerating voltage of 5 KV and working distance is 6 nm. The XRPD diffractograms of Ni NPs were recorded on Siemens D5000 X-ray diffractometer using Cu kα radiations, whereas the particle size was determined using PicoPlus AFM of Agilent Technologies. Sample preparation for AFM involved making a solution of Ni NPs in acetone, spreading it over Si substrate and evaporating the acetone, thus leaving behind just Ni NPs on Si Substrate. For magnetic hysteresis, 10–20 mg sample powder was packed in butter paper and measurements were taken at room temperature using a vibrating sample magnetometer (VSM).

Results and discussion

The complexes tris(2,2′-bipyridine)nickel(II) chloride, $[Ni(2,2'\text{-bipy})_3]Cl_2{\cdot}5H_2O$ (**1**), and bis(2,2′-bipyridine) nickel(II) chloride, $[Ni(2,2'\text{-bipy})_2Cl_2]$ (**2**) were prepared

by reported methods [27, 28] and characterized by melting point, UV/Vis, CHN, ^{1}H-NMR, and mass spectrometry. The complexes (**1**) and (**2**) show λ_{max} at 534 and 600 nm, respectively, and all other analytical data obtained for both the complexes are in good agreement with that reported in the literature [28, 29].

Thermogravimetric data of the complexes (**1**) and (**2**) suggested that under inert atmosphere, both the complexes finally degrade to Ni(0) along with the elimination of various volatile by-products. This decomposition to Ni(0) proceeds by four steps (Figs. 1, 2) that are not well defined indicating that formation of unstable moieties is taking place during degradation process. In case of (**1**) early decomposition (at <200 °C) started probably with release of water of coordination resulting in mass loss of 31.06% followed by second step that commensurate to mass loss of 37.15%. Further, two-step decomposition yields the final residue of 6.02%, which is identified as zero-valent Nickel (ZVN). A slight mass loss was observed between 600 and 900 °C which might be due to the elimination of traces of residual carbon. An identical degradation pattern was observed by complex (**2**) except that its decomposition starts at 200 °C owing to its higher stability as compared to (**1**) which was attributed to the absence of water of coordination (Fig. 2). The first step results in mass loss of 24.74% followed by three successive indistinctive steps showing elimination of bipyridine, hydrogen chloride, and chlorine in different stages with mass loss of 22.63 and 19.41% giving final residue of 7.29% that corresponds to ZVN. On the other hand, hydrated $NiCl_2$ is found to be stable up to 400 °C above which it decomposes in the presence of inert atmosphere by dehydrochlorination, dechlorination, and partial oxidation [30].

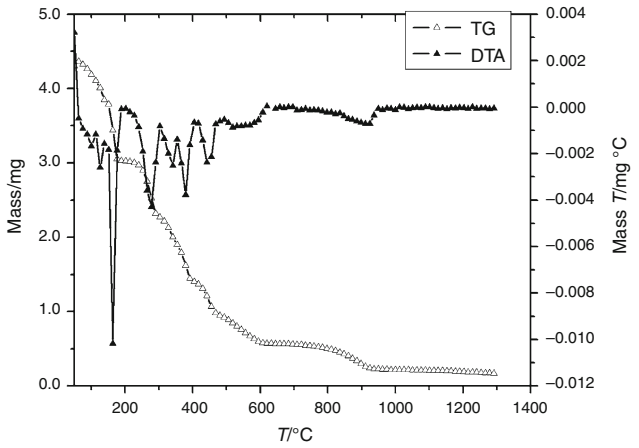

Fig. 1 TG and DTA curves of tris(bipyridine)nickel(II) chloride (**1**) taken at 5 °C/min heating rate and 50 mL/min flow rate of Ar gas

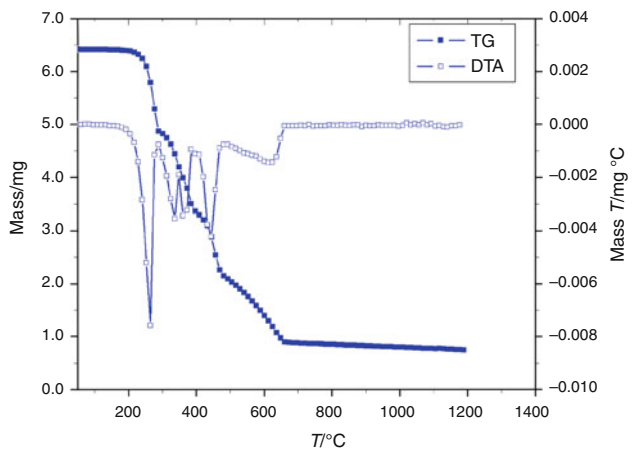

Fig. 2 TG and DTA curves of bis(bipyridine)nickel(II) chloride (**2**) taken at 5 °C/min heating rate and 50 mL/min flow rate of Ar gas

In order to confirm our findings and determine the nature of by-products released during the degradation of complexes, various experiments were conducted in tube furnace at 450 °C under inert atmosphere of flowing argon gas at different heating rates. It showed that decomposition carried out at heating rate of 50 °C/min had negligible contamination of carbon, hydrogen, and nitrogen. GC–MS analysis of the trapped gases evolved from exhaust of the tube furnace helped in elucidation of simple degradation mechanism (Scheme 1). The evolved gases were found to contain bipyridine as a major constituent as confirmed by GC–MS, which shows a peak at retention time of 5.561 min having *m*/*z* value of 156 (Fig. 3). Except bipyridine, no other major stable by-product having molecular mass greater than bipyridine was identified in the mass spectra (Fig. 3) as also indicated by TG curve. Though low-molecular-weight unstable specie was observed having *m*/*z* 51 corresponding to $C_4H_3^+$ moiety, which is formed by cleavage of bipyridine ring.

No peak was observed for 6-chlorobipyridine, bipyridine hydrochloride, or 6,6′-dichlorobipyridine in GC–MS evolved gas analysis as was observed in earlier studies for similar iron complex [31]. The removal of chloride from the complexes (**1**) and (**2**) and hence its presence in evolved

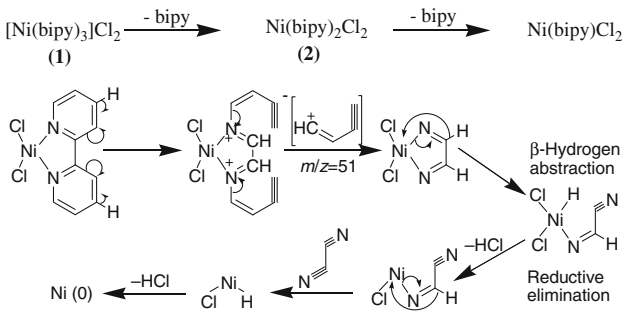

Scheme 1 Proposed mechanism for thermal decomposition of complexes (**1**) and (**2**) to Ni(0) nanoparticles

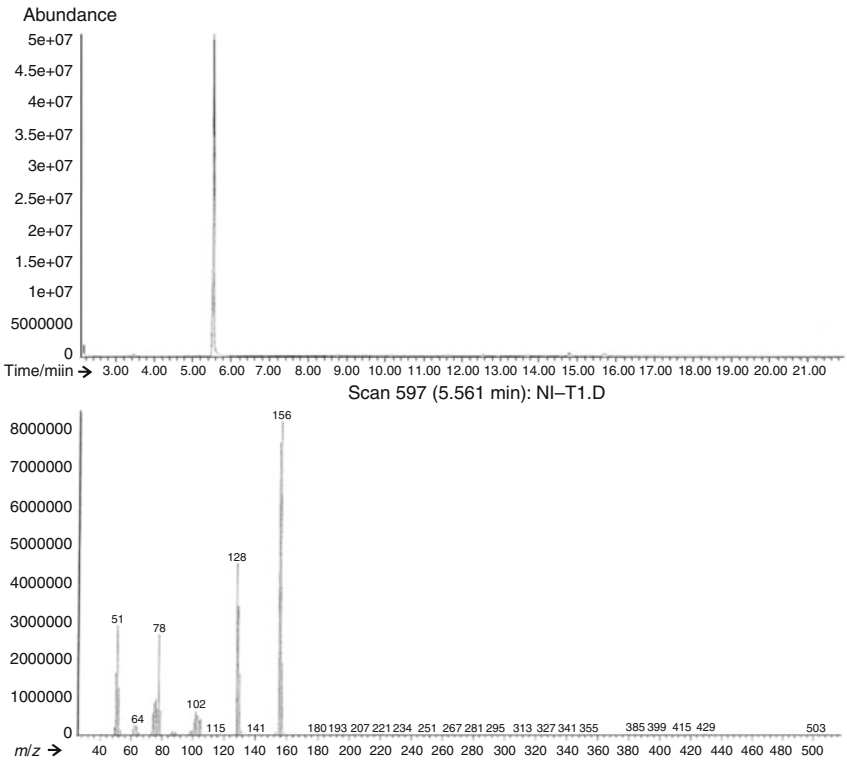

Fig. 3 GC–MS studies of evolved gas obtained by thermal degradation of complex (1) (*top*) showing peak at retention time of 5.61 min along with its MS fragmentation pattern (*bottom*) confirming bipyridine as major by-product

gases was assured by the appearance of turbidity in silver nitrate bath owing to the formation of silver chloride as a result of reaction between hydrogen chloride coming from reaction vent with silver nitrate [32].

Based on our observations and GC–MS analysis, a mechanism (Scheme 1) is proposed for thermal degradation of complexes (**1**) and (**2**) to Ni(0). Thermal decomposition of complex (**1**) starts with elimination of bipyridine that results in the formation of (**2**). Further removal of bipyridine from (**2**) causes coordinative unsaturation on Ni(0) center that paved the way to the formation of ZVN by elimination reactions of successive unstable intermediates (Scheme 1). These unstable intermediates, identified by GC–MS, result from simple rearrangement of bipyridine ring prior to β-hydrogen abstraction by nickel center followed by reductive elimination.

The thermal stability of residue of Ni particles obtained after thermal decomposition of complexes (**1**) and (**2**), i.e., Ni-1 and Ni-2, respectively, was checked by recording their TG in the temperature range of 100–1300 °C (Fig. 4). A minute loss in mass was observed that indicates stability of particles under experimental conditions. CHN and EDX analysis of the particles showed <3% of carbon and nitrogen containing impurity. Further experiments had shown that these impurities can be removed by increasing the argon gas flow rate, which helps in wiping out the by-products released during pyrolysis from the reaction chamber and hence reducing their chances of combination to give stable polymeric product.

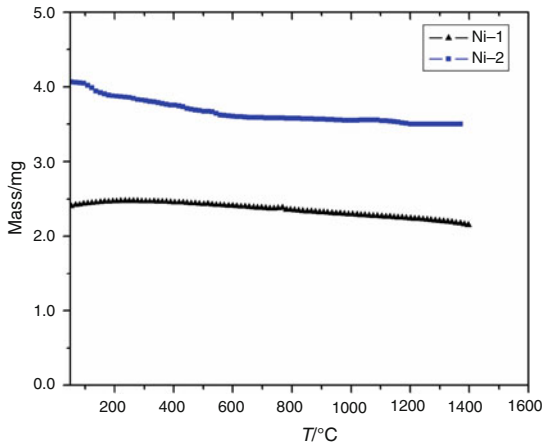

Fig. 4 TG curves of residue Ni-1and Ni-2 obtained after thermolysis of complexes (**1**) and (**2**) taken at 5 °C/min heating rate and 50 mL/min flow rate of Ar gas

Nickel NPs, Ni-1, and Ni-2, residue obtained by thermal decomposition of bipyridine complexes (**1**) and (**2**) were subjected to various other analyses in order to confirm their nature. XRPD diffractograms (Fig. 5) of the residue (Ni-1 and Ni-2) indicate the formation of pure *fcc* Ni as no additional diffraction peaks due to other phases were identified in the pattern. The peaks were indexed successfully on the basis of *fcc* Ni as shown in insets of Fig. 5.

Formation of particles in nano-range was confirmed by AFM analysis of thin film of NPs prepared using spin coating. It was shown that thermolysis of (**1**) at heating rate

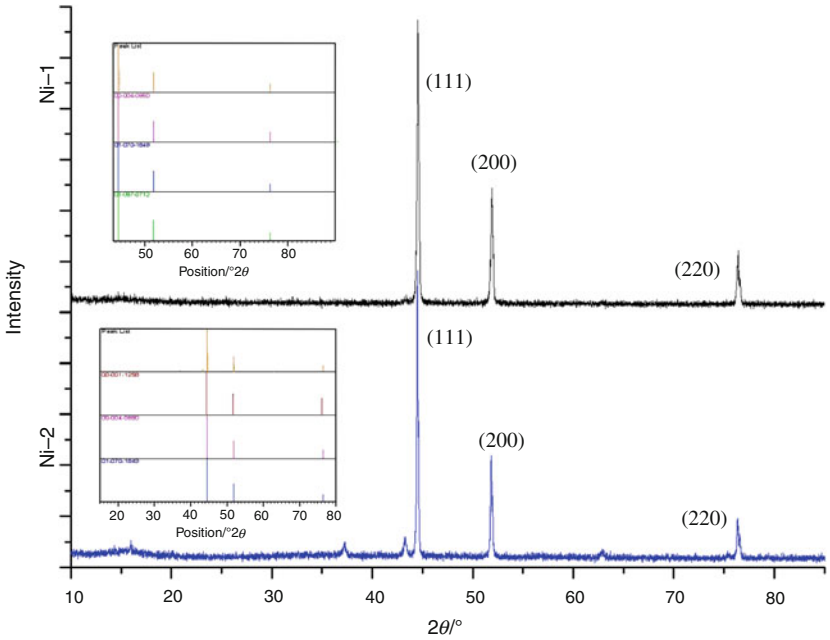

Fig. 5 XRPD diffractograms of Ni-1 showing matching with CCDC 00-004-0850, 01-070-1849, and 01-087-0712 in inset and Ni-2 showing matching in inset with CCDC 00-001-1258, 00-004-0850, and 01-070-1849

of 50 °C/min generates the NPs (Ni-1) with an average particle size (PS) of 3.5 nm, while under identical conditions, the larger particles (Ni-2) having an average size of 5.0 nm are obtained via thermolysis of (**2**), as shown in Fig. 6. Thus, by simply changing the precursor, nanoparticles of various sizes can be obtained. Early but comparatively slow decomposition of (**1**) as compared to (**2**) (as indicated by TG curve, Figs. 1, 2) might have attributed to the formation of smaller particles. Also, in case of bulky molecules like (**1**), chances of aggregation are reduced; hence, particles tend to remain smaller with less coagulation that finally resulted in smaller particles as compared to the comparatively less bulky complex (**2**).

Thus, nanoparticles of different sizes can be obtained by exploiting the nature of the precursor used. In addition to that, particle size can also be varied by changing the heating rates employed for thermal decomposition of complexes. In the present study, various independent experiments were carried out for thermal decomposition of the two complexes at two different heating rates, i.e., 1 °C/min and 50 °C/min. It was observed that smaller particles are obtained in each case when complexes (**1**) and (**2**) were decomposed at heating rate of 50 °C/min as compared to the ones that were obtained at lower heating rate, i.e., 1 °C/min. At lower heating rates, there are more chances of particles' aggregation, which on other hand becomes less feasible when higher heating rates are used. Also, at higher heating rates, attainment of thermal decomposition temperature (450 °C) is rapid, which cause fast and speedy decomposition of precursors and elimination of decomposition by-products to result in ZVN.

In order to study the magnetic properties of the prepared Ni NPs, Ni-1, and Ni-2, hysteresis plots were recorded at room temperature, which point toward the ferromagnetic

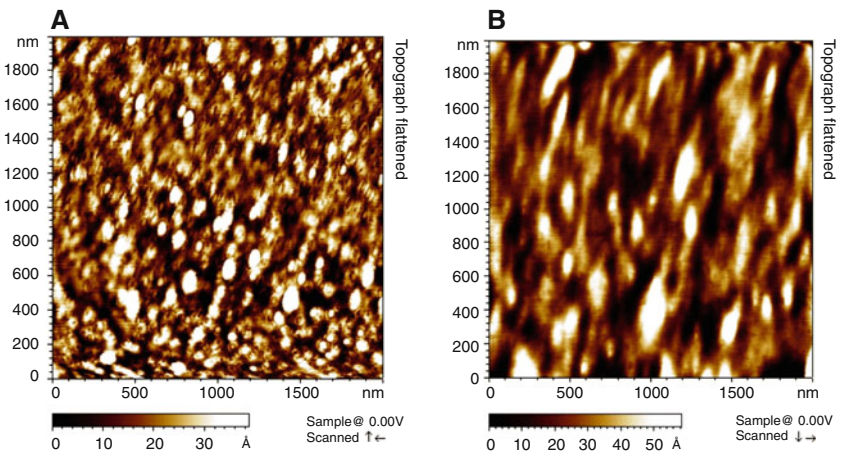

Fig. 6 AFM images of Ni nanoparticles; **a** Ni-1 and **b** Ni-2 showing particle size of 3.5 and 5.0 nm, respectively

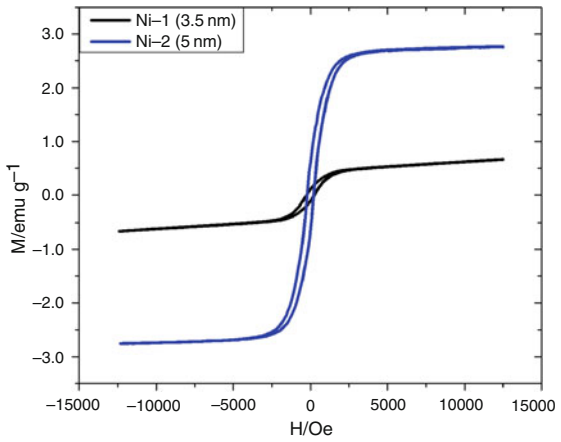

Fig. 7 M-H plot of Ni-1 and Ni-2 having *fcc* structure showing ferromagnetic behavior with enhanced coercivity

Table 1 Parameters of magnetic hysteresis recorded at room temperature for Ni-1 and Ni-2

Sample code	PS/nm	H_C/Oe	M_R/emu g^{-1}	M_S/emu g^{-1}
Ni-1	3.5	254.61	0.103	0.662
Ni-2	5.0	210.92	0.644	2.758

nature of both the samples as evident from the Fig. 7. Both the samples show coercivity, H_C, of 254 Oe and 210 Oe (Table 1), which is much higher than that of the bulk Ni (0.7 Oe) [33] and is comparable to that of bulk Fe (220 Oe) [34, 35].

Increase in coercivity is usual for small particles, and it increases with decrease in particle size. The reason for this is attributed to the formation of single domain particles as with decrease in size, formation of domains no longer remain feasible. Consequently, in these single domain particles, rotation of magnetization is much more difficult than in bulk system having domains [34, 35]. But on the other hand, these single domain particles can be easily magnetized; hence, resulting in considerable reduction in saturation magnetization, M_S, which in turn decreases as the particle size decreases [36]. This is also observed in the present case where M_S reduces from 2.758 to 0.662 emu/g as the particle size decreases from 5.0 to 3.5 nm, which is much lower than that observed in case of bulk (55 emu/g). Reduction in M_S of Ni NPs, i.e., 31.40 to 27.7 emu/g with decrease in particle size from 5.0 to 3.8 nm had also been observed earlier in magnetic hysteresis collected at low temperature and high field [36, 37].

Hence, ZVN NPs having *fcc* structure with appreciable coercivity can be prepared by simple thermochemical approach that also enables control of particle size that in turn control the magnetic properties of the sample synthesized.

Conclusions

Face-centered cubic-phased Ni(0) NPs with controlled shape and average size of 3.5–5.0 nm can be synthesized via thermal decomposition of tris(bipyridine)nickel(II) chloride (**1**) and bis(bipyridine)nickel(II) chloride (**2**) under inert atmosphere of flowing argon gas. Based on GC–MS analysis of the evolved gas, a thermal breakdown mechanism of the complexes to ZVN NPs has been worked out. It has been inferred that by careful selection of the precursor, control of heating and argon gas flow rates, different sized NPs can be prepared. Magnetic hysteresis studies show ferromagnetic nature of Ni NPs with coercivity comparable to that of bulk iron.

Acknowledgements MM is grateful for financial support from HEC, Pakistan, through grant no. 1-308/ILPUF and HIR/UMRG grant no. UM.C/625/1/1/6 and RG097/10AET University of Malaya, Malaysia.

References

1. Kung HH, Kung MC. Nanotechnology: applications and potentials for heterogeneous catalysis. Catal Today. 2004;97:219–24.
2. Mackowiecka M, Kepinski L, Jurczyk M. Nanoscale hydrogen storage materials studied by TEM. Rev Adv Mater Sci. 2008; 18:621–6.
3. Tungler A. Thermal methods in the investigation of nickel catalysts. J Therm Anal Calorim. 2005;79:521–4.
4. Arayne S, Sultana N. Review: nanoparticles in drug delivery for the treatment of cancer. Pak J Pharm Sci. 2006;19:258–68.
5. Verrelli E, Tsoukalas D, Giannakopoulos K, Kouvatsos D, Normand P, Ioannou DE. Nickel nanoparticles deposition at room temperature for memory applications. Microelectron Eng. 2007;84:1994–7.
6. Hu Y, Yu Y, Zhao X, Yang H, Feng B, Li H, Qiao Y, Hua L, Pan Z, Hou Z. Catalytic hydrogenation of aromatic nitro compounds by functionalized ionic liquids-stabilized nickel nanoparticles in aqueous phase: the influence of anions. Sci China Chem. 2010;53:1541–8.
7. Metin O, Özkar S, Sun S. Monodisperse nickel nanoparticles supported on SiO_2 as an effective catalyst for the hydrolysis of ammonia-borane. Nano Res. 2010;3:676–84.
8. Boudjahem A, Monteverdi S, Ghanbaja D, Bettahar MM. Nickel nanoparticles supported on silica of low surface area. Hydrogen chemisorptions and TPD and catalytic properties. Catal Lett. 2002;84:115–22.
9. Hou Y, Kondoh H, Ohta T, Gao S. Size-controlled synthesis of nickel nanoparticles. Appl Surf Sci. 2005;241:218–22.
10. Jia FL, Zhang LZ, Shang XY, Yang Y. Non-aqueous sol-gel approach towards the controllable synthesis of nickel nanospheres, nanowires and nanoflowers. Adv Mater. 2008;20:1050–4.
11. Zhang DE, Ni XM, Zheng HG, Li Y, Zhang XJ, Yang ZP. Synthesis of needle-like nickel nanoparticles in water-in-oil microemulsion. Mater Lett. 2005;59:2011–4.
12. Ni X, Su X, Yang Z, Zheng H. The preparation of nickel nanorods in water-in-oil microemulsion. J Cryst Growth. 2003;252: 612–7.
13. Chen D, Liu S, Li J, Zhao N, Shi C, Du X. Nanometer Ni and core/shell Ni/Au nanoparticles with controllable dimensions

synthesized in reverse microemulsion. J Alloys Compd. 2009;475:494–500.
14. Duan H, Lin X, Liu G, Xu L, Li F. Synthesis of Ni nanoparticles and their catalytic effect on the decomposition of ammonium perchlorate. J Mater Process Technol. 2008;208:494–8.
15. Kim S, Yoo BK, Chun K, Kang W, Choo J, Gong M, Joo S. Catalytic effect of laser abalated Ni nanoparticles in the oxidative addition reaction for coupling reagent of benzylchloride and bromoacetonitrile. J Mol Catal A Chem. 2005;226:231–4.
16. Couto GG, Klein JJ, Schreiner WH, Mosca DH, de Oliveira AJA, Zarbin AJG. Nickel nanoparticles obtained by a modified polyol process: synthesis, characterization, and magnetic properties. J Colloid Interf Sci. 2007;311:461–8.
17. Eastoe J, Hollamby MJ, Hudson L. Recent advances in nanoparticles synthesis with reverse micelles. Adv Colloid Interface Sci. 2006;128–130:5–15.
18. Davar F, Fereshteh Z, Salavati-Niasari M. Nanoparticles of Ni and NiO: synthesis, characterization and magnetic properties. J Alloys Compd. 2009;476:797–801.
19. Domínguez-Crespo MA, Ramírez-Meneses E, Montiel-Palma V, Huerta AMT, Rosales HD. Synthesis and electrochemical characterization of stabilized nickel nanoparicles. Int J Hydrog Energy. 2009;34:1664–76.
20. Armit HW. The toxicology of Nickel carbonyl. J Hyg. 2009;7:525–51.
21. Luo X, Chen Y, Yue G, Peng D, Luo X. Preparation of hexagonal close-packed nickel nanoparticles vis a thermal decomposition approach using nickel acetate tetrahydrate as a precursor. J Alloys Compd. 2009;476:864–8.
22. Rejitha KS, Mathew S. Thermal behaviour of nickel(II) suphate, nitrate and halide complexes containing ammine and ethylenediamine as ligands: kinetics and evolved gas analysis. J Therm Anal Calorim. 2011;106:267–75.
23. Rejitha KS, Ichikawa T, Mathew S. Thermal decomposition studies of $[Ni(NH_3)_6]X_2$ (X = Cl, Br) in the solid state using TG-MS and TR-XRD. J Therm Anal Calorim. 2011;103:515–23.
24. Kim S, Terashi Y, Purwanto A, Okuyama K. Synthesis and film deposition of Ni nanoparticles for base metal electrode applications. Colloid Surf A. 2009;337:96–101.
25. Goto Y, Taniguchi K, Omata T, Otsuka-Yao-Matsuo S. Formation of Ni_3C nanocrystals by thermolysis of nickel acetylacetonate in oleylamine: characterization using hard X-ray photoelectron spectroscopy. Chem Mater. 2008;20:4156–60.
26. Mourdikoudis S, Simeonidis K, Vilalta-Clemente A, Tuna F, Tsiaoussis I, Angelakeris M. Controlling the crystal structure of Ni nanoparticles by the use of alkylamines. J Magn Magn Mater. 2009;321:2723–8.
27. Ruiz-Pérez C, Luis PAL, Lloret F, Julve M. Dimensionally controlled hydrogen-bonded nanostructures: synthesis, structure, thermal and magnetic behavior of the tris-(chelated)nickel(II) complex $[Ni(bipy)3]Cl_2{\cdot}5H_2O$ (bipy = 2,2′-bipyridyl). Inorg Chim Acta. 2002;336:131–6.
28. Haris CM, Mckenzie ED. Nitrogenous chelate complexes of transition metals-III: bis-chelate complexes of nickel (II) with 1,10-phenanthroline, 2,2-bipyridyl and analogous ligands. J Inorg Nucl Chem. 1967;29:1047–68.
29. Závoianu R, Nenu C, Angelescu E. Ni(2,2′-bipyridine)2Cl2 encapsulated in Y zeolite new catalyst for ethylene dimerization. Catal Commun. 2005;6:415–20.
30. Mishra SK, Kanungo SB. Thermal degradation and decomposition of nickel chloride hydrate ($NiCl_2{\cdot}xH_2O$). J Therm Anal Calorim. 1992;38:2417–36.
31. Nazir R, Mazhar M, Wakeel T, Akhtar MJ, Siddique M, Nadeem M, Khan NA, Shah MR. Pyrolysis mechanism of trisbipyridine-iron(II) chloride to iron nanoparticles. J Therm Anal Calorim 2011. doi:10.1007/s10973-011-1919-5.
32. Svehla G. Vogel's qualitative inorganic analysis. 7th ed. India: Dorling Kindersley (Pvt.) Ltd; 1996.
33. Narayanan TN, Shaijumon MM, Ajayan PM, Anantharaman MR. Synthesis of high coercivity core-shell nonorods based on nickel and cobalt and their magnetic properties. Nanoscale Res Lett. 2010;5:164–8.
34. Çelebi O, Üzüm Ç, Shahwan T, Erten HN. A radiotracer study of the adsorption behavior of aqueous Ba^{2+} ions on nanoparticles of zero-valent iron. J Hazard Mater. 2007;148:761–7.
35. Klabunde KJ. Nanoscale materials in chemistry. New Jersey: Wiley; 2009.
36. Sahoo Y, He Y, Swihart MT, Wang S, Luo H, Furlani EP, Prasad PN. An aerosol-mediated magnetic colloid: study of nickel nanoparticles. J Appl Phys 2005. doi:10.1063/1.2033145.
37. Hou Y, Gao S. Monodisperse nickel nanoparticles prepared from a monosurfactant system and their magnetic properties. J Mater Chem. 2003;13:1510–2.